OPEN ACCESS
JOURNAL OF ADVANCED DIELECTRICS
Vol. 12, No. 2 (2022) 2150030 (7 pages)

DOI: 10.1142/S2010135X21500302

Hydrothermal synthesis of $ABi_2Ta_2O_9$ Aurivillius phase: A comparative study of A-site cation size on structure, dielectric, optical properties

Ilona Bella*, Tio Putra Wendari*, Novesar Jamarun*, Nandang Mufti† and Zulhadjri*,‡

*Department of Chemistry, Universitas Andalas, Kampus Limau Manis, Padang 25163, Indonesia

†Center of Advanced Materials for Renewable Energy, Universitas Negeri Malang
Jl. Semarang 5, Malang 65145, Indonesia

‡zulhadjri@sci.unand.ac.id

Received 8 October 2021; Revised 16 November 2021; Accepted 1 December 2021; Published 15 December 2021

In this study, the double-layered Aurivillius phases $CaBi_2Ta_2O_9$ (CBT) and $PbBi_2Ta_2O_9$ (PBT) were prepared through a hydrothermal route with NaOH as a mineralizer. XRD analysis confirmed that the CBT and PBT compounds were successfully formed and adopted an orthorhombic crystal structure with an $A2_1am$ symmetry. Le Bail refinements of XRD data indicated that the unit cell volume of CBT was smaller than PBT and is associated with the smaller ionic radius of Ca^{2+} compared to Pb^{2+}. The surface morphology of both samples, as determined using SEM, demonstrated plate-like grains with anisotropic grain growth. It was found that the different ionic radii of *A*-site cations (Ca^{2+} and Pb^{2+}) strongly affected the structural, optical and electrical properties of the Aurivillius phase. The occupation of smaller Ca^{2+} cations induced a higher structural distortion, which resulted in higher bandgap (E_g) energy and ferroelectric transition temperature (T_c) of CBT, compared to those of PBT.

Keywords: Aurivillius phase; hydrothermal synthesis; Le Bail refinement; relaxor-ferroelectric; anisotropic grain; optical properties.

1. Introduction

In the past few decades, perovskite-structured ferroelectrics have received exponentially increasing attention, primarily due to their appealing physical properties such as high dielectric permittivity, diffuse phase transition and piezoelectric properties.[1–3] They have also been applied successfully in a variety of electronic applications, including multilayer capacitors, sensors, actuators, transducers, energy storage and memory applications.[4–6] Aurivillius phases have recently attracted considerable interest for this multifunction because they are ferroelectric and possess a large remanent polarization and a low leakage current. Aurivillius compounds have gained increasing attention towards the development of renewable energy sources for solar cell and electrocaloric (EC) cooling systems.[7,8]

Structurally, the Aurivillius phases can be considered as layered intergrowths of fluorite-like $[Bi_2O_2]^{2+}$ layers alternating with *n*-perovskite-like $[A_{n-1}B_nO_{3n+1}]^{2-}$ layers stacking along the *c*-axis. The *A* typically represents monovalent, divalent, or trivalent cations with 12-fold coordination (e.g., Na^+, Ca^{2+}, Pb^{2+}, Ba^{2+}, Sr^{2+}, Ln^{3+}) and *B* represents a transition metal cation with 6-fold coordination (e.g., Ti^{4+}, Nb^{5+}, Ta^{5+}, W^{6+}).[9] The electrical properties of the Aurivillius phase have been thoroughly investigated in terms of the effect of $6s^2$ lone-pair electrons and the ionic radii of *A*-site cations constructing the Aurivillius structure. The substitution of the *A*-site cation results in a change in the *B*–O bond distance and angles, and the latter affects the electrical properties of these materials, to some extent.[10,11]

To date, solid-state reaction is the most common method for producing Aurivillius phases. However, the volatilization of Bi^{3+} frequently occurs at a high temperature, which tends to form impurities and requires the addition of excess Bi_2O_3 in synthesis procedures.[12,13] This drawback can be overcome by using soft chemical methods such as the hydrothermal method, which involves heating a liquid-phase reaction medium and precursors in an autoclave at a low temperature and high pressure.

The benefits of this particular route will produce the fine particles with a narrow size distribution which is well known with the compositional and particle homogeneity that significantly affects the physical properties Aurivillius phases.[14–16] However, there are a limited number of studies on the hydrothermal preparation of CBT and PBT powders in the literature.

Herein, the double-layer Aurivillius phases $CaBi_2Ta_2O_9$ and $PbBi_2Ta_2O_9$ were prepared using a hydrothermal route that had not previously been reported in the related literature. Furthermore, a comparative study was carried out on different sizes of *A*-site cation (Ca^{2+} and Pb^{2+}) ions on structure,

‡Corresponding author.

morphology, dielectric and optical properties. The Ca^{2+} was chosen to represent the smallest *A*-site cation usually used. Meanwhile, the Pb^{2+} is a cation with $6s^2$ lone pair electrons since their ionic characteristic was expected to induce a highly distorted structure and high ferroelectricity in the Aurivillius family phases.

2. Experimental Details

The polycrystalline samples of Aurivillius CBT and PBT phases were prepared by a hydrothermal route using $CaCO_3$, PbO, Bi_2O_3 and Ta_2O_5 (Aldrich, ≥ 99.9%) as precursors. Stoichiometric amounts of the precursors were added in 60 ml NaOH 3 M under continuous stirring for 2 h. The solution was transferred into a 100 ml teflon lined stainless steel autoclave reactor and then heated at 240°C for 120 h. After being cooled to room temperature, the precipitates were filtered and washed with deionized water until a pH of 7 was obtained. The products were dried at 110°C for 6 h and calcined at 550°C for 5 h and 900°C for 4 h. The phase and structural determinations were performed by X-ray Diffraction technique (XRD; X'Pert3 Powder PANalytical, Cu-Kα radiation). The crystal structure unit cells were investigated using the Le Bail refinement technique using the RIETICA program.[17] Room temperature FTIR spectra were collected on a Perkin Elmer 1600 FTIR spectrophotometer. The grain morphology and size were observed by a scanning electron microscope (SEM; Hitachi Flexsem 1000). The powders were mixed with a 5 wt.% PVA binder and subsequently dried pressed into pellets. The pellet samples were sintered at 900°C for 5 h in a muffle furnace. The sintered pellets were then coated with silver conductive paste (Aldrich, 99%) on both sides for use as electrodes. The capacitance and dielectric loss were measured by using an LCR meter (BK Precision 891) in the frequency range of 50–300 kHz at various temperatures.

3. Results and Discussion

Figure 1 depicts the room temperature XRD patterns of the Aurivillius samples $ABi_2Ta_2O_9$ (A = Ca^{2+}, Pb^{2+}) prepared by the hydrothermal method XRD patterns of both samples. The figure demonstrates an orthorhombic $A2_1am$ structure that could be assigned to those double-layered Aurivillius $CaBi_2Ta_2O_9$ (ICSD-93754), indicating that the double-layered Aurivillius phase was successfully formed. Moreover, the highest intensity of (1 1 5) diffraction peak represented the double-layer Aurivillius phases with m = 2, which was consistent with the fact that the strongest reflection of the perovskite-type phases was all of the types of (1 1 2m+1).[18] Compared with Pb^{2+} ions (1.49 Å), Ca^{2+} ions (1.34 Å) had a smaller ionic radius.[19] These characteristics resulted in higher 2θ for the 115 peaks observed for the CBT sample. In contrast, the peak of the PBT sample appeared at lower angles, as shown in the enlarged XRD patterns. This phenomenon

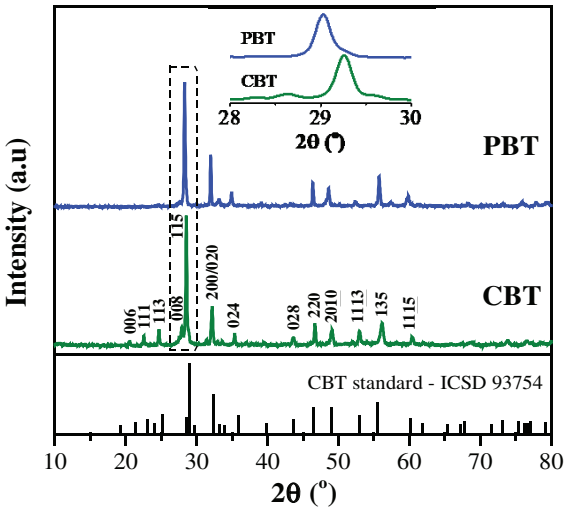

Fig. 1. XRD patterns of CBT and PBT samples indexed according to the standard double-layer Aurivillius phase CBT with $A2_1am$ space group.

could be evidence of variations in the lattice parameters and distortion of each crystal structure.[20]

Further analysis of the crystal structure was analyzed by the Le Bail refinement technique on the XRD data. The lattice parameters of the orthorhombic $A2_1am$ structure of CBT (a = 5.466 Å, b = 5.432 Å, c = 24.962 Å, ICSD-93754) and PBT (a = 5.496 Å, b = 5.469 Å, c = 25.553 Å, ICSD-95920) were used as the initial structure models. The background, unit cell and profile were refined to produce the best Le Bail profile and the satisfactory reliability factors (R_p, R_{wp}, χ^2), as shown in Fig. 2. The Le Bail plots of both samples show that the observed XRD pattern was well-matched with the calculated patterns, and all diffraction peaks were fitted with the Bragg reflection for space group $A2_1am$. These results demonstrate that the synthesized CBT and PBT phases substitution adopted an orthorhombic $A2_1am$ structure.[21]

The effects of different sizes of *A*-site cation on crystal structure that were further observed from the refined lattice parameters are listed in Table 1. All lattice parameters with the unit cell volume of PBT were larger than CBT, which were consistent with the larger ionic radius of Pb^{2+} (1.49 Å) compared to Ca^{2+} (1.34 Å), for 12-fold coordination in the perovskite layers.[19] Furthermore, the orthorhombic distortion associated with the changed values of the a and b lattice parameters became crucial to investigate, which was related to the electrical properties of the Aurivillius phase.[22] In the double-layered Aurivillius phase with the $A2_1am$ space group, the octahedral distortion occurred in the perovskite layer was determined by the relative tilting and rotation angles between two neighboring BO_6 octahedra along the c-axis, leading to a larger difference in the a and b lattice parameters and an increased orthorhombicity ratio.[10,23] Theoretically, this octahedra distortion can be quantified as orthorhombicity ratio ($(a - b)/(a + b)$) shown in Table 2. The orthorhombicity of

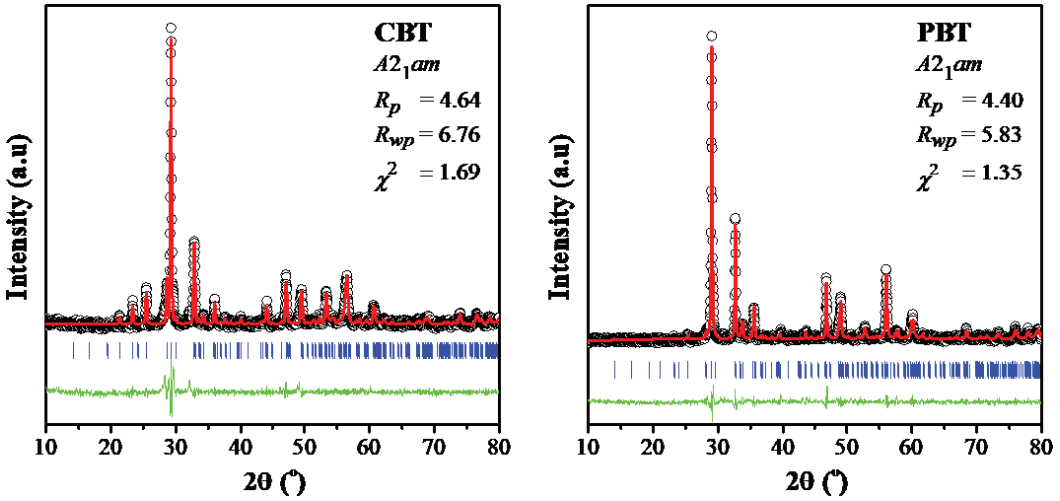

Fig. 2. Le Bail refinement profile of Aurivillius CBT and PBT samples using the $A2_1am$ space group.

Table 1. Refined structural parameters of CBT and PBT samples obtained from Le Bail refinements using XRD data.

	$CaBi_2Ta_2O_9$	$PbBi_2Ta_2O_9$
Space group	$A2_1am$	$A2_1am$
Crystal class	Orthorhombic	Orthorhombic
a (Å)	5.4570(4)	5.5173(1)
b (Å)	5.4297(2)	5.5262(6)
c (Å)	24.9138(5)	25.622(4)
V (Å^3)	738.192(2)	781.218(1)
(a – b)/(b – a)	0.0273	0.0089
Z	4	4
R_p (%)	4.48	4.81
R_{wp} (%)	6.04	5.71
χ^2	0.675	0.701

Table 2. Variation of electrical properties of samples measured at 300 kHz.

Sample	ε_{RT}	tan δ (RT)	T_c(°C)	ε_m	tan δ (T_m)	(a – b)/(a + b)	t
PBT	141.24	0.0294	550	251.54	0.0774	0.0089	0.971
CBT	67.36	0.0197	> 900	—	—	0.0273	0.945

CBT was larger than that of PBT, which implies that the perovskite-part structure of CBT had a more distorted orthorhombic structure. The smaller Ca^{2+} ions in CBT caused higher compressive stress in the perovskite unit, which induced the mismatch between the perovskite layer and the Bi_2O_2 layer. Besides, these findings resulted in a significant distortion in the TaO_6 octahedra.[20] This trend in structural distortion can also theoretically explain the Goldschmidt tolerance factor (t) for the perovskite part of the Aurivillius structure which was calculated using the following equation:

$$t = \frac{R_A + R_B}{\sqrt{2}(R_B + R_O)}, \quad (1)$$

where R_A, R_B and R_O were the ionic radii for the A-site cation, B-site cation and oxygen ion, respectively. The t value for CBT was 0.945 which was smaller than that of PBT (0.971). It was noted that the higher structural distortion in CBT was due to the occupation of smaller Ca^{2+} cations on the A-site and one of the possible reasons for the enhancement of the ferroelectric transition temperature (T_c).[24]

The effects of the A-site ionic size on structural changes were investigated using FTIR. Figure 3 shows the room temperature IR spectra of CBT and PBT samples in the range of 550–900 cm^{-1}. In Fig. 3, both samples exhibit two vibration modes around ~595 cm^{-1} and ~783 cm^{-1}, corresponding to the

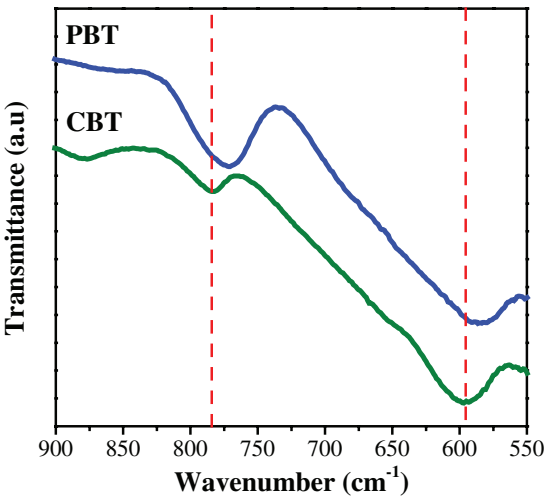

Fig. 3. Room temperature IR spectra of CBT and PBT powder samples.

vibration of symmetric Ta–O stretching and asymmetric Ta–O stretching of the TaO_6 octahedra, respectively. We focused on these vibration modes since the characteristic vibrations of the Ta–O bond in TaO_6 octahedra are strongly correlated to the origin of structural distortion.[25] Essentially, this mode should be identical since the different *A*-site cations (Ca^{2+} and Pb^{2+}) did not occupy the TaO_6 structure. However, a slight difference in wavenumber observed in Fig. 3 was induced by the different sizes of *A*-site cation in the perovskite block, leading to a difference in TaO_6 octahedra size,[26] as revealed by refinement analysis. These vibration modes of the CBT sample appeared at higher wavenumbers of ~597 cm^{-1} and ~783 cm^{-1}, compared to PBT (584 cm^{-1} and 770 cm^{-1}). It is known that the shifting of modes toward a higher wavenumber is proportionally affected by the reduced mass and stronger bond strength of the bonded atoms.[27] Compared to PBT, the occupation of smaller Ca^{2+} resulted in a shorter Ta–O bond with smaller lattice parameters, thereby raising the bond strength, and giving rise to the vibration mode at higher wavenumbers.

The grain morphologies of CBT and PBT powder samples observed by an SEM are depicted in Fig. 4. Anisotropic grains with plate-like morphologies with no pores in the grains were found in both samples which is considered a grain growth characteristic in the Aurivillius phases.[28,29] The particle size was analyzed by ImageJ software and is approximately in the range of 0.11–0.928 μm for CBT, and was found to be larger (around 0.074–1.726 μm) for PBT. It is also observed that the grains differ in size, which could be attributed to the different ionic radii of the *A*-site cation, resulting in a smaller CBT particle size.[30] It is noted that the hydrothermal route has resulted in the relatively uniform and smaller grain size compared to the high-temperature method.[31] It is well known that temperature has more influence on grain growth, the higher temperature during annealing process leads to increase the crystallinity of the material and hence increases the number of crystallites.

The optical band gap energy (E_g) of the CBT and PBT was deduced from the UV-Vis diffuse reflectance spectra by applying the Tauc's plots between $(\alpha h\upsilon)^2$ versus $h\upsilon$.[32] The E_g was estimated from the intersection of the linear fits of the Tauc's plot to $(\alpha h\upsilon)^2 = 0$. The estimated E_g value of CBT was 3.38 eV, which was higher than PBT, as shown in Fig. 5. The E_g value was closely related to the structural distortion effect generated due to the different sizes of the *A*-site cations. Previous studies found that the decreasing size of the *A*-site cations resulted in higher E_g energy in the perovskite-based compounds.[30,33] Theoretically, the high bond strength in a semiconductor material is derived from the strongly-bound valence electrons, thus limiting a complete charge transfer. Therefore, the smaller Ca^{2+} cation in CBT results in a higher structural distortion and bond strength in TaO_6 octahedra, showing the shift of the valence band (VB) to higher energies and inducing larger E_g.

Figure 6 presents the temperature dependence of the dielectric constant (ε) and dielectric loss (tan δ) at a high-frequency range of 50–300 kHz to investigate the relationship between the structural and the electrical properties.[34] For CBT, the magnitude of the ε gradually increased with an increase in temperature until the maximum temperature range of 900°C. Meanwhile, the T_c peak in CBT was not observed over the

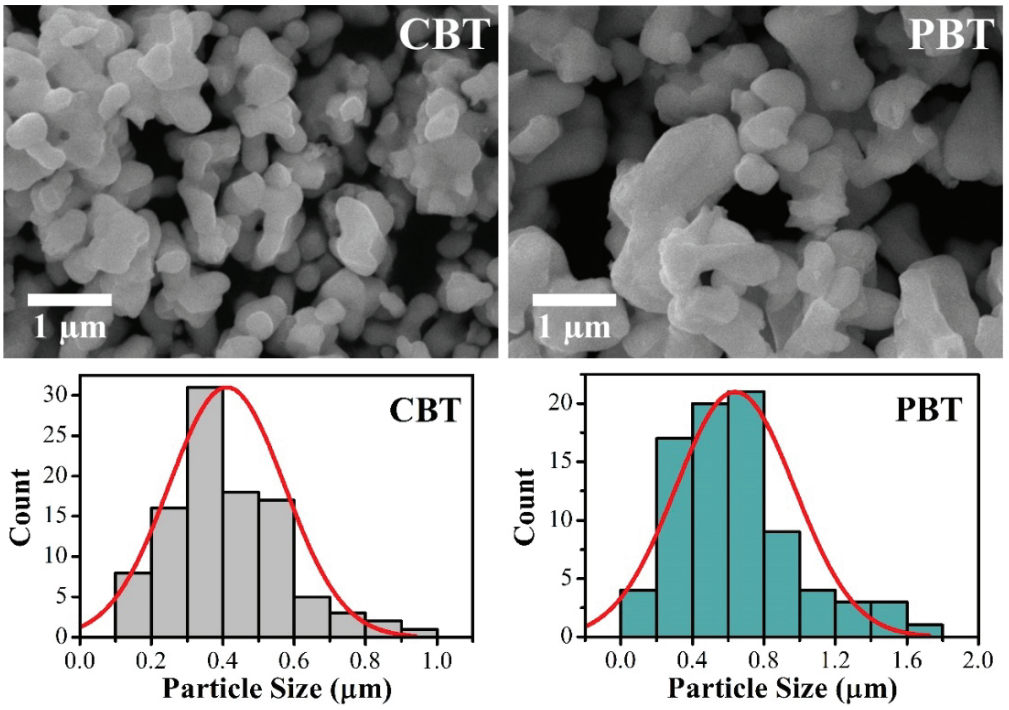

Fig. 4. SEM micrographs and particle size distribution of CBT and PBT powder samples.

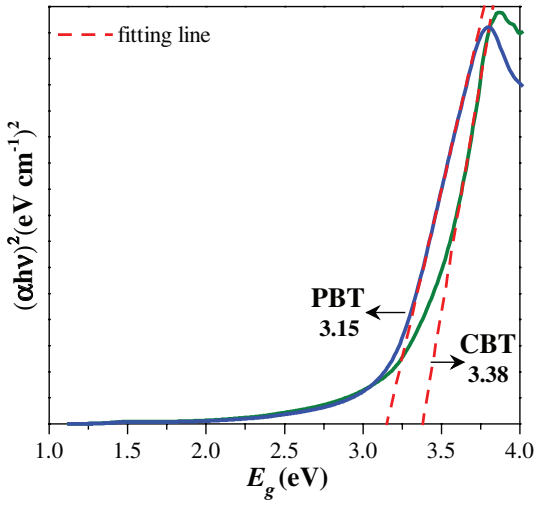

Fig. 5. Tauc's plots of CBT and PBT samples for determination of the optical bandgap energy (E_g).

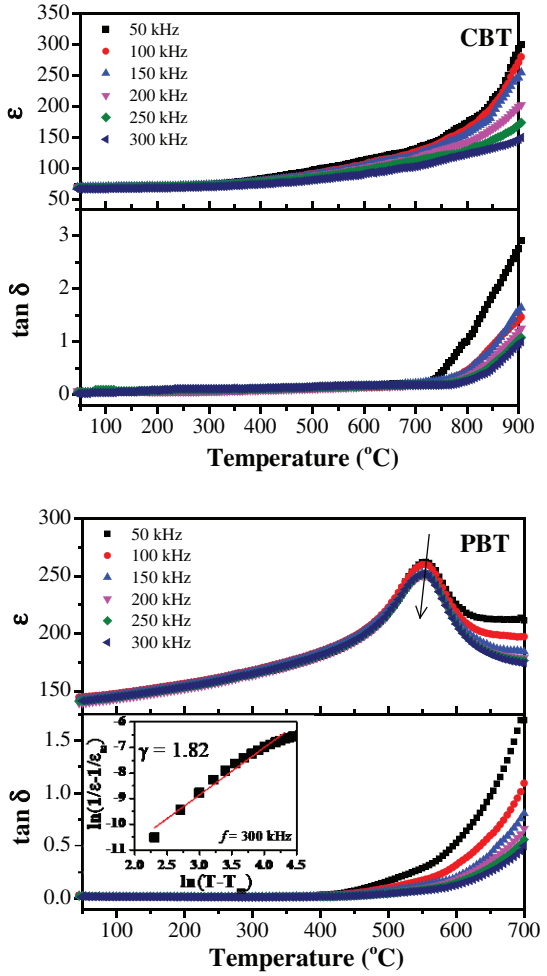

Fig. 6. Temperature and frequency dependence of dielectric constant (ε) and dielectric loss (tan δ) of CBT and PBT samples. The inset figure represents a modified Curie–Weiss fitted curve for PBT.

temperature range, suggesting the T_c was higher than that temperature, which exceeded the high-temperature limit of our instrument setup. At higher temperatures, the silver paste as the electrodes was heat damaged, so no electrical conductivity occurred. It was reported that the $CaBi_2Ta_2O_9$ is a normal ferroelectric phase with a sharp dielectric constant peak of 923°C.[35] Compared to CBT, a single peak in the dielectric constant of the PBT sample was observed at 550°C, which is the well-defined ferroelectric-paraelectric phase transition temperature (T_c).[11] This T_c reveals the predominance of the ferroelectric phase for both compounds in the range of RT to temperature below T_c, according to a noncentrosymmetric orthorhombic structure with the $A2_1am$ space group. Moreover, the dielectric loss of PBT increases significantly at the temperature above T_c, which can also indicate a transition to the paraelectric phase where the sample becomes more conducting. A higher T_c in the Ca-based Aurivillius phase had been widely reported compared to other A-site cations (Pb^{2+}, Sr^{2+} and Ba^{2+}). Since the Ca^{2+} cation has the smallest ionic radius, it induces the greatest BO_6 octahedra distortion and results in the highest T_c.[25,29] These phenomena were also revealed by the higher distortion degree and tolerance factor, as discussed in the structural analysis above.

Moreover, the magnitude of the dielectric constant at room temperature of PBT was larger than CBT, as listed in Table 2. This phenomenon should be proportional to the grain size, which was also considered the driving force for the formation of the domain walls. Since the grain size of PBT was larger (see Fig. 4), the motion of the domain walls became easier, and the sample was more easily polarized, contributing to a higher magnitude.[28]

The dielectric loss was found to be low and stable at temperatures below the T_c, suggesting that both samples have high dielectric stability, which is important for high-temperature device applications. It is also noted that the increased number of grain boundaries as a decrease in the grain size restricted the electron transports, which led to a lower dielectric loss in CBT.[39] The dielectric loss value in CBT also indicates a lower electrical conduction process, which reflects the phenomenon of charge conduction inhibition due to a larger optical band gap.

Interestingly, PBT samples exhibited a broader peak of dielectric constant, accompanied by frequency-dispersive behavior, indicating the characteristic of the relaxor-ferroelectric phase.[8,36] The dielectric peaks at 50 kHz and 300 kHz exhibited a slight shift of 5°C (ΔT relaxation), related to the existence of ferroelectric nanodomain motion in the relaxor phase. The degree of diffuseness (γ) calculated from the modified Curie–Weiss law equation can also be used to evaluate the relaxor behavior.[37]

$$\frac{1}{\varepsilon_r}-\frac{1}{\varepsilon_m}=\frac{(T-T_m)^{\gamma}}{C}, \tag{2}$$

where ε_m denotes the maximum dielectric constant at the transition temperature, C denotes the Curie–Weiss constant,

and γ denotes the degree of relaxor behavior. Thus, the γ value can be obtained by linear fitting between $\ln(1/\varepsilon_r - 1/\varepsilon_m)$ versus $\ln(T - T_m)$, where $\gamma = 1$ expresses a normal ferroelectric behavior and $\gamma = 2$ expresses a relaxor behavior. The obtained γ value at 300 kHz, as shown in the inset of Fig. 6. The obtained γ value of PBT was 1.87, implying that this sample became a relaxor ferroelectric phase.

Typically, the relaxor behavior was believed to originate from the disorder of various cations at the same crystallographic positions.[36] According to previous studies on the $PbBi_2Nb_2O_9$ phase, the Bi^{3+} and Pb^{2+} cations have a similar preference to disorder over the *A*-site of the perovskite layer and the Bi_2O_2 layer since both cations possess a stereochemical active $6s^2$ lone pair electrons and a similar ionic size.[10,38] The broad dielectric peak with the ΔT relaxation of 5°C induced by the disorder phenomenon in the $PbBi_2Nb_2O_9$ was relevant to the current PBT sample in this work.[10] Thus, the disordered Pb^{2+} and Bi^{3+} cations on both the bismuth and perovskite layers were most likely to blame for this behavior in the PBT sample. The disorder induced the breakdown of long-range-ordered ferroelectric macrodomains into polar nanoregions (PNRs), resulting in relaxor behavior.[21,37]

4. Conclusions

The hydrothermal route was used to synthesis the double-layered Aurivillius phase $CaBi_2Ta_2O_9$ (CBT) and $PbBi_2Ta_2O_9$ (PBT). According to XRD analysis, both samples were successfully formed and had a noncentrosymmetric orthorhombic with $A2_1am$ symmetry. The SEM micrographs of the powder samples show plate-like grain morphologies with highly anisotropic grain growth, which is a characteristic of the Aurivillius phase. The structural analysis of XRD, combined with the refinement method and FTIR, revealed that the structural distortion of CBT was higher than of PBT, as the influence of the smaller ionic size had a significant impact on both electrical and optical properties. Additionally, relaxor ferroelectric behavior was observed in the PBT sample, driven by the disorder of Pb^{2+}/Bi^{3+} cations on the *A*-site of the Bi_2O_2 and perovskite layers.

Acknowledgments

This research was funded through PMDSU Scholarship Grant No. 050/SP2H/LT/DRPM/2018 sponsored by the Ministry of Research, Technology and Higher Education (RISTEKDIKTI) of The Republic of Indonesia.

References

[1]J. F. Scott, *Ferroelectric Memories*, 1st edn. (Springer-Verlag Berlin Heidelberg, New York, 2000).
[2]W. Gao, Y. Zhu, Y. Wang, G. Yuan and J. M. Liu, A review of flexible perovskite oxide ferroelectric films and their application, *J. Mater*. **6**, 1 (2020).
[3]L. Yang, X. Kong, F. Li, H. Hao, Z. Cheng, H. Liu, J.F. Li and S. Zhang, Perovskite lead-free dielectrics for energy storage applications, *Prog. Mater. Sci*. **102**, 72 (2019).
[4]L. Zhu, J. Zhou, Z. Guo and Z. Sun, An overview of materials issues in resistive random access memory, *J. Mater*. **1**, 285 (2015).
[5]U. De, K. R. Sahu and A. De, Ferroelectric materials for high temperature piezoelectric applications, *Solid State Phenom*. **232**, 235 (2015).
[6]A. Manan, M. U. Rehman, A. Ullah, A. S. Ahmad, Y. Iqbal, I. Qazi, M. A. Khan, H. U. Shah and A. H. Wazir, High energy storage density with ultra-high efficiency and fast charging-discharging capability of sodium bismuth niobate lead-free ceramics, *J. Adv. Dielectr*. **11**, 1 (2021).
[7]M. Valant, A. K. Axelsson, F. Le Goupil and N. M. N. Alford, Electrocaloric temperature change constrained by the dielectric strength, *Mater. Chem. Phys.* **136**, 277 (2012).
[8]A. K. Axelsson, F. Le Goupil, M. Valant and N. M. N. Alford, Optimisation of $SrBi_2(Nb,Ta)_2O_9$ Aurivillius phase for lead-free electrocaloric cooling, *J. Eur. Ceram. Soc*. **38**, 5354 (2018).
[9]B. Aurivillius, Mixed bismuth oxides with layer lattices 1. The Structure type of $CaNb_2Bi_2O_9$, *Ark. För Kemi*. **1**, 463 (1949).
[10]T. P. Wendari, S. Arief, N. Mufti, A. Insani, J. Baas, G. R. Blake and Zulhadjri, Structure-property relationships in the lanthanide-substituted $PbBi_2Nb_2O_9$ Aurivillius phase synthesized by the molten salt method, *J. Alloys Compd*. **860**, 158440 (2021).
[11]X. Zeng, F. Cao, Z. Peng and X. Xing, Crystal structure and electrical properties of (Li, Ce,Nd)-multidoped $CaBi_2Nb_2O_9$ high temperature ceramics, *Ceram. Int*. **44**, 3069 (2018).
[12]X. He, R. Chu, Z. Xu, Z. Yao and J. Hao, Effect of Bi_2O_3 content on the microstructure and electrical properties of $SrBi_2Nb_2O_9$ piezoelectric ceramics, *RSC Adv*. **8**, 15613 (2018).
[13]C. Qin, Z. Y. Shen, W. Q. Luo, F. S. Song, Y. Hong, Z. M. Wang and Y. M. Li, Effect of excess Bi on the structure and electrical properties of $CaBi_2Nb_2O_9$ ultrahigh temperature piezoceramics, *J. Mater. Sci. Mater. Electron*. **29**, 7801 (2018).
[14]Z. Xu, R. Chu, J. Hao, Z. Yao and H. Li, Hydrothermal preparation and electrical properties of Aurivillius phase $SrBi_4Ti_4O_{15}$ ceramic, *Ferroelectrics* **516**, 148 (2017).
[15]M. Afqir, A. Tachafine, D. Fasquelle, M. Elaatmani, J. Carru and A. Zegzouti, Structural and dielectric properties of $SrBi_{2-x}Ce_xNb_2O_9$ ($0 \le x \le 0.35$) ceramics, *J. Electron. Mater.* **47**, 5793 (2018).
[16]H. Chen, B. Shen, J. Xu, L. Kong and J. Zhai, Correlation between grain sizes and electrical properties of $CaBi_2Nb_2O_9$ piezoelectric ceramics, *J. Am. Ceram. Soc.* **95**, 3514 (2012).
[17]B. A. Hunter, *Rietica – A Visual Rietveld Program* (Australian Nuclear Science and Technology Organisation, Australia, 2000).
[18]M. Afqir, A. Tachafine, D. Fasquelle, M. Elaatmani, J. Carru, A. Zegzouti and M. Daoud, Synthesis, structural and dielectric properties of $SrBi_{2-x}La_xNb_2O_9$ ceramics prepared by hydrothermal treatment, *Appl. Phys. A* **124**, 83 (2018).
[19]R. D. Shannon, Revised effective ionic radii and systematic studies of interatomie distances in halides and chaleogenides, *Acta Cryst*. **32**, 751 (1976).
[20]Y. Li, G. Chen, H. Zhang, Z. Li and J. Sun, Electronic structure and photocatalytic properties of $ABi_2Ta_2O_9$ (A = Ca, Sr, Ba), *J. Solid State Chem*. **181**, 2653 (2008).
[21]I. Bella, T. P. Wendari, N. Jamarun, N. Mufti and Zulhadjri, Structural transformation in Mn-substituted $Sr_2Bi_2Ta_2TiO_{12}$ Aurivillius phase synthesized by hydrothermal method: A comparative study and dielectric properties, *Ceram. Int.* **47**, 8014 (2020).
[22]A. B. Missyul, I. A. Zvereva, T. T. M. Palstra and A. I. Kurbakov, Double-layered Aurivillius-type ferroelectrics with magnetic moments, *Mater. Res. Bull*. **45**, 546 (2010).
[23]K. S. Aleksandrov and J. Bartolomé, Structural distortions in families of perovskite-like crystals, *Phase Transit*. **74**, 255 (2001).

[24]S. Moharana, S. Sai and R. N. Mahaling, Enhanced dielectric and ferroelectric properties of surface hydroxylated $Na_{0.5}Bi_{0.5}TiO_3$ (NBT)-poly(vinylidene fluoride) (PVDF) composites, *J. Adv. Dielectr*. **8**, 19 (2018).

[25]V. D. Phadtare and V. R. Puri, Studies on electrical and dielectric properties of co-precipitated Aurivillius phase $Ca_{1-x}Ba_xBi_2Nb_2O_9$ ceramics, *Ceram. Int*. **42**, 8581 (2016).

[26]A. Prasetyo, B. Mihailova, V. Suendo, A. A. Nugroho and Ismunandar, The effect of the A-Site cation on the structural transformations in $ABi_4Ti_4O_{15}$ (A= Ba, Sr): Raman scattering studies, *J. Solid State Chem*. **283**, 121131 (2020).

[27]C. L. Diao, H. W. Zheng, Y. Z. Gu, W. F. Zhang and L. Fang, Structural and electrical properties of four-layers Aurivillius phase $BaBi_{3.5}Nd_{0.5}Ti_4O_{15}$ ceramics, *Ceram. Int.* **40**, 5765 (2014).

[28]T. P. Wendari, S. Arief, N. Mufti, J. Baas, G. R. Blake and Zulhadjri, Ratio effect of salt fluxes on structure, dielectric and magnetic properties of La,Mn-doped $PbBi_2Nb_2O_9$ Aurivillius phase, *Ceram. Int.* **46**, 14822 (2020).

[29]Z. Yao, R. Chu, Z. Xu, J. Hao, D. Wei and G. Li, Dielectric, ferroelectric and piezoelectric properties of $Ca_{0.1}Sr_{0.9}Bi_2Nb_2O_9$ ceramic, *J. Mater. Sci. Mater. Electron*. **26**, 8740 (2015).

[30]P. Nayak, K. Mitra and S. Panigrahi, Electrical and optical properties of four-layered perovskite ferroelectric $ABi_4Ti_4O_{15}$ (with A = Sr, Ba, Ca), *Mater. Lett*. **216**, 54 (2018).

[31]S. L. Rasheed and E. K. Al-Shakarchi, The nanostructure of barium dititanate prepared by hydrothermal method, *J. Adv. Dielectr*. **9**, 1 (2019).

[32]D. Wang, K. Tang, Z. Liang and H. Zheng, Synthesis, crystal structure, and photocatalytic activity of the new three-layer aurivillius phases, $Bi_2ASrTi_2TaO_{12}$ (A=Bi,La), *J. Solid State Chem*. **183**, 361 (2010).

[33]R. Prasanna, A. Gold-Parker, T. Leijtens, B. Conings, A. Babayigit, H. G. Boyen, M. F. Toney and M. D. McGehee, Band gap tuning via lattice contraction and octahedral tilting in perovskite materials for photovoltaics, *J. Am. Chem. Soc*. **139**, 11117 (2017).

[34]Z. Zulhadjri, A. A. Billah, T.P. Wendari, E. Emriadi, U. Septiani and S. Arief, Synthesis of aurivillius phase $CaBi_4Ti_4O_{15}$ doped with both La^{3+} and Mn^{3+} Cations: Crystal structure and dielectric properties, *Mater. Res*. **23**, 2 (2020).

[35]D. Peng, X. Wang, C. Xu, X. Yao, J. Lin and T. Sun, Bright upconversion luminescence and increased Tc in $CaBi_2Ta_2O_9$:Er high temperature piezoelectric ceramics, *J. Appl. Phys*. **111**, 104111 (2012).

[36]M. Zhang, X. Xu, Y. Yue, M. Palma, M. J. Reece and H. Yan, Multi elements substituted Aurivillius phase relaxor ferroelectrics using high entropy design concept, *Mater. Des*. **200**, 109447 (2021).

[37]Z. Peng, X. Xing, X. Zeng, Y. Xiang, F. Cao and B. Wu, High performance of La, Nd multi-rare earth doped $Na_{0.46}Li_{0.04}Bi_{2.5}Nb_2O_9$ high temperature piezoceramics at a new pseudo-MPB, *Mater. Res. Bull*. **97**, 393 (2018).

[38]Ismunandar, B. A. Hunter and B. J. Kennedy, Cation disorder in the ferroelectric Aurivillius phase $PbBi_2Nb_2O_9$: An anamolous dispersion X-ray diffraction study, *Solid State Ion*. **112**, 281 (1998).

[39]X. Tian, S. Qu, H. Ma, Z. Pei and B. Wang, Effect of grain size on dielectric and piezoelectric properties of bismuth layer structure $CaBi_2Nb_2O_9$ ceramics, *J. Mater. Sci. Mater. Electron*. **27**, 1 (2016).